J. Applied Membrane Science & Technology, Vol. 30, April 2026, 1-22

Knudsen Number Sensitivity to Pressure Drop in Composite Ceramic Membranes

Muktar M. Ramalan[1]*, Idris Hashim[2], Muhammad Dauda[3], Igbagara Tonye[4]

[1]School of Computing, Engineering and Technology, Robert Gordon University, Aberdeen, United Kingdom
[2]School of Computing, Engineering and Technology, Robert Gordon University, Aberdeen, United Kingdom
[3]Department of Mechanical Engineering, Ahmadu Bello University, Zaria, Nigeria
[4]School of Computing, Engineering and Technology, Robert Gordon University Aberdeen, United Kingdom

Submitted: 03/11/2025. Revised edition: 27/11/2025. Accepted: 02/12/2025. Available online: 21/04/2026

ABSTRACT

Gas transport in nanoscale ceramic membranes is fundamentally governed by the Knudsen number (Kn), which differentiates between molecular dominated and continuum dominated flow regimes. This study experimentally evaluates the sensitivity of Kn to transmembrane pressure across multilayer alumina membranes comprising a 15 nm selective layer, a 200 nm intermediate layer, and a 6000 nm macroporous support. Hydrogen (H_2), carbon dioxide (CO_2), and air were investigated at 100 °C over a pressure range of 20–300 kPa. The results consistently show an inverse relationship between Kn and pressure for all gases and pore sizes, as predicted by kinetic gas theory due to the pressure dependent decrease in molecular mean free path. Among the gases studied, hydrogen exhibits the strongest pressure sensitivity in the 15 nm layer, followed by CO_2 and air, reflecting differences in molecular size and diffusivity. Linear regression applied to the experimental Kn–ΔP trends yields coefficients of determination of $R^2 \approx 0.8875$ across all gases and pore diameters, confirming high linearity and strong internal consistency in the measurements. Although the R^2 values remain constant, each gas exhibits a distinct regression slope and intercept, as shown in Figures 4–6, indicating differing Kn pressure response characteristics. Complementary SEM and dynamic wettability measurements further support the mechanistic interpretation. The 15 nm top layer shows the highest hydrophilicity (equilibrium contact angle ≈ 60°), promoting enhanced gas–wall interactions. The 200 nm layer exhibits intermediate wettability (≈ 70°), while the 6000 nm support is weakly hydrophobic (≈ 93°). These structural and surface properties help explain the observed trends: smaller and more hydrophilic pores intensify molecule–wall collisions, amplifying Knudsen-dominated transport. Overall, the findings provide validated experimental benchmarks for modelling rarefied gas transport in composite ceramic membranes, with implications for hydrogen purification, CO_2 separation, and catalytic membrane reactor design.

Keywords: Knudsen number; ceramic nanomaterials; mean free path; hydrogen separation; contact angle

* Corresponding to: M. M. Ramalan (email: mukramaramalan@gmail.com)
DOI: https://doi.org/10.11113/jamst.v30n1.335

1.0 INTRODUCTION

Porous membranes have gained considerable attention due to their ability to selectively transport gases and liquids with high efficiency and tunability. Ceramic composite membranes, in particular, offer superior chemical stability, thermal resistance, and mechanical strength compared with polymeric alternatives, making them attractive for hydrogen purification, carbon capture, catalytic reactions, and ammonia synthesis. Their performance, however, is governed by nanoscale transport phenomena that often deviate from classical continuum assumptions.

A fundamental parameter describing gas transport in porous materials is the Knudsen number (Kn), defined as the ratio of molecular mean free path (λ) to the characteristic pore diameter (dp). Kn identifies the governing transport regime continuum ($Kn < 0.1$), transition ($0.1 < Kn < 10$), or free molecular ($Kn > 10$). As pore size decreases or pressure is reduced, gas-wall collisions become increasingly dominant, producing Knudsen or transitional flow behaviour. Accurately quantifying how Kn varies with transmembrane pressure is therefore essential for predicting membrane permeance and selectivity under practical operating conditions.

Theoretical descriptions based on Knudsen diffusion and the dusty-gas model (DGM) integrate molecular diffusion, viscous flow, and multicomponent interactions, providing a basis for modelling transport across a wide range of pressures and pore sizes [1–5]. Recent image-based and microstructural characterisation approaches have significantly refined these models by linking effective transport parameters to real membrane morphologies [6–8]. However, there remains limited experimental validation particularly for multilayer ceramic membranes composed of hierarchical pore structures. Most earlier studies focus on single pore systems or idealised geometries, leaving uncertainty in how real composite membranes behave across the transition regime.

Experimental advances such as high-vacuum diffusion cells and precision pressure-drop systems now enable direct measurements of Knudsen and transitional transport [9–11]. Yet, comparative studies across multiple pore sizes, gas species, and operating pressures are still scarce, limiting the ability to validate models or derive design-relevant scaling laws. This gap is especially significant for modern ceramic membranes, which often incorporate thin selective layers (sub-50 nm) deposited on meso- or macroporous supports to create multilayer composite architectures [12–19]. Such structures combine several transport regimes in series, making it essential to understand how Kn responds within each layer.

Correlating pore structure and surface properties with transport behaviour has become increasingly important. SEM and EDX analyses offer insight into pore geometry, interconnection, and layer continuity [20–23], while time-resolved contact-angle measurements reveal surface energy and wettability, both of which influence gas–solid interactions [24-26]. Despite these tools, a quantitative, experimentally validated relationship between pore geometry, surface wettability, and Kn–pressure sensitivity across hierarchical ceramic membranes has not been clearly established. Most prior studies treat pore geometry or surface chemistry independently, without coupling both under controlled multilayer conditions [27-28]. Furthermore, many studies consider only a single gas species, which limits relevance for hydrogen purification, CO_2 capture, and air separation processes requiring multi-gas comparisons [29–32].

* Corresponding to: M. M. Ramalan (email: mukramaramalan@gmail.com)
DOI: https://doi.org/10.11113/jamst.v30n1.335

The hierarchical pore architecture of real ceramic membranes introduces coupled Knudsen and viscous transport dynamics that cannot be captured using uniform-pore models. Understanding how Kn sensitivity varies with pressure across pore sizes ranging from tens of nanometres to several micrometres is therefore essential for establishing reliable transport scaling across the rarefied continuum spectrum [33- 35].

1.1 Research Gap and Novelty

This study fills these gaps by experimentally quantifying the sensitivity of the Knudsen number ($\Delta Kn/\Delta P$) to transmembrane pressure in a multilayer ceramic composite membrane comprising 15 nm, 200 nm, and 6000 nm pore scale layers, using hydrogen, carbon dioxide, and air at 100 °C. By correlating Kn trends with SEM morphology and time-resolved contact-angle measurements, this work establishes a mechanistic relationship between pore geometry, surface wettability, and rarefied-flow behaviour.

Specifically, the study provides the first systematic experimental demonstration that:

1. Kn pressure sensitivity ($\Delta Kn/\Delta P$) scales inversely with pore size, with smaller pores exhibiting stronger rarefaction effects due to enhanced gas wall collision frequency.
2. Hydrophilic, high surface energy nanopores amplify gas wall interactions and adsorption under transitional flow conditions, resulting in stronger deviations from ideal kinetic predictions.
3. Coupled analysis of pore geometry and surface wettability explains the differing Kn sensitivities across hierarchical membrane lay**ers**, providing a mechanistic framework unavailable in prior experimental studies.

These findings bridge the gap between theoretical transport models and real membrane architectures, advancing understanding of nanoscale gas transport in hierarchical ceramic membranes. The insights gained enable rational design of selective membranes and membrane-assisted catalytic systems for hydrogen energy, carbon capture, and environmental separations.

2.0 EXPERIMENTAL

2.1 Membrane Materials and Structure

The experimental study was performed using multilayer tubular inorganic ceramic membranes fabricated from high purity alumina. Each membrane consisted of a layered support structure comprising macroporous inner layers and progressively smaller pores toward the outer selective layer. Three representative pore sizes were investigated 15 nm, 200 nm, and 6000 nm. The 15 nm layer served as the outermost selective coating to provide enhanced gas discrimination, while the 200 nm and 6000 nm inner layers acted as mechanical supports to maintain structural integrity under differential pressure. This multilayer configuration represents a typical composite ceramic design widely adopted for gas separation and catalytic membrane reactor applications.

* Corresponding to: M. M. Ramalan (email: mukramaramalan@gmail.com)
DOI: https://doi.org/10.11113/jamst.v30n1.335

The effective permeable length of the tubular supports ranged from 378 to 665 mm, with total tube lengths of 446 mm (200 and 6000 nm supports) and 733 mm (15 nm membranes). All membranes were sintered to produce stable porous structures with well-defined pore diameters. Prior to testing, the membranes were oven-dried at 120 °C for 12 h to eliminate residual moisture and ensure reproducible surface conditions.

2.2 Gases and Experimental Conditions

Three representative gases were selected: hydrogen (H_2), carbon dioxide (CO_2), and air chosen to encompass a broad range of molecular masses, kinetic diameters, and industrial relevance in hydrogen energy and CO_2 capture systems. Each gas was supplied from high purity laboratory cylinders (BOC Ltd., purity > 99.99 %). Composition certificates confirmed impurity levels below 0.01 % for hydrogen and within ± 2 % for nitrogen/oxygen balance gases.

All experiments were conducted at a controlled temperature of 100 °C, maintained using a thermostatically regulated heating system wrapped uniformly around the membrane housing. This ensured thermal stability across the entire permeation pathway and prevented localised temperature gradients that could influence gas transport behaviour. The choice of a fixed temperature was deliberate: although the molecular mean free path (and therefore the Knudsen number) scales with temperature through kinetic theory, varying temperature would introduce an additional variable that complicates direct comparison of pressure driven Knudsen responses across the three pore size layers. By holding temperature constant, the study isolates the influence of transmembrane pressure and pore diameter on Kn sensitivity, ensuring that observed differences arise solely from pressure variations and membrane microstructure.

During operation, the transmembrane pressure was varied incrementally between 0.2 and 3.0 bar (20–300 kPa absolute), while the permeate side was held constant at 1 atm (101.3 kPa) to maintain a well defined and reproducible pressure gradient. At each pressure step, the system was allowed to stabilise for at least 15 minutes before recording steady state readings. This stabilisation period minimised transient flow effects, thermal drift and fluctuations in gas density. Although temperature dependent effects such as changes in gas viscosity and mean free path are relevant to Knudsen-dominated transport, these were intentionally excluded from the present study to maintain experimental clarity. A systematic investigation of combined temperature pressure interactions is recommended for future work, particularly for membranes operating under elevated temperature conditions in industrial applications.

2.3 Experimental Setup

Gas permeation measurements were performed in a radial-flow configuration (Figure 1a), in which the feed gas entered the shell side of the tubular membrane and permeated radially through the multilayer wall into the lumen. This arrangement ensured that the selective 15 nm layer was directly exposed to the feed stream, while the underlying mesoporous and macroporous layers provided mechanical support. The permeate gas was collected at the tube exit, and the retentate was vented to atmosphere.

* Corresponding to: M. M. Ramalan (email: mukramaramalan@gmail.com)
DOI: https://doi.org/10.11113/jamst.v30n1.335

The experimental assembly consisted of the following principal components:

1. Compressed gas cylinder and dual stage pressure regulator for controlled feed delivery.
2. High pressure stainless steel line conveying the feed gas to the test module.
3. Inlet pressure gauge and digital manometer for accurate measurement of feed pressure.
4. Membrane housing containing the tubular sample mounted vertically within a steel holder.
5. Heating jacket and thermocouple network for maintaining a uniform operating temperature along the membrane surface.
6. Outlet pressure gauge and relief valve venting the permeate stream to atmospheric exhaust.
7. Data-acquisition system (digital logger) for monitoring pressure and temperature continuously during each run.

During operation, gas flowed in sequence through the numbered components in Figure 1a: regulated feed delivery (1–3), controlled heating and permeation through the membrane module (4–5), and discharge through the outlet and measurement section (6), while pressure and temperature profiles were recorded in real time (7). Pressure was measured using calibrated transducers (±0.25% F.S.), temperature using K-type thermocouples (±1 °C), and gas flow rates using digital mass-flow meters (±2% uncertainty).

Figure 1b provides a complementary schematic of the internal test module configuration. After passing through the regulator and gauges, the conditioned feed gas enters the steel core holder containing the porous membrane sample (labelled as the "porous core"). The gas fills the annular shell region surrounding the membrane, ensuring that the selective outer surface is fully exposed to the feed stream, radial permeation occurs through the selective layer.

Heating tape wrapped around the core holder maintains a consistent operating temperature, controlled via an external heat regulator and monitored by thermoprobes and a digital thermometer. At the outlet, the permeate gas passes through a calibrated flow meter before being discharged safely to a fume cupboard. End-seals within the core holder prevent bypass flow and ensure that all gas transport occurs strictly through the membrane wall. Together, Figures 1a and 1b illustrate the full gas-delivery path, uniform heating arrangement, radial permeation geometry, and measurement points used to obtain reliable Knudsen-number and pressure drop data.

2.4 Data Processing and Calculations

The transmembrane pressure drop (ΔP) was obtained as the difference between inlet and outlet absolute pressures, converted to pascals using the relation 1 bar = 1 × 10^5 Pa. The mean free path of gas molecules (λ) was determined using the kinetic theory expression:

$$\lambda = \frac{KT}{\sqrt{2\pi}d^2P} \quad (1)$$

where k is the Boltzmann constant, T is the operating temperature (373 K), d is the

* Corresponding to: M. M. Ramalan (email: mukramaramalan@gmail.com)
DOI: https://doi.org/10.11113/jamst.v30n1.335

molecular collision diameter, and P is the absolute pressure. The Knudsen number was then calculated as:

$$Kn = \frac{\lambda}{d_p} \quad (2)$$

where d_p is the characteristic pore diameter (15 nm, 200 nm, or 6000 nm).

The molecular parameters for each gas including collision diameter, molar mass, and viscosity were obtained from established literature sources. Each test condition was performed in triplicate to ensure reproducibility, and the resulting deviations in calculated Kn values remained within ±5%, indicating strong internal consistency. Linear regression analysis of Kn versus pressure produced coefficients of determination of $R^2 = 0.886 \pm 0.002$, demonstrating a highly linear relationship between rarefaction effects and pressure for all gas pore combinations. To verify the reliability of the calculated Kn values, theoretical Kn–pressure curves based on kinetic gas theory were also generated for comparison. A detailed discussion of the agreement between experimental and theoretical trends is presented in Section 3.3

2.5 The Influence of Parameters Knudsen Number

Although porosity, gas viscosity, and membrane thickness strongly affect the overall gas transport behaviour through porous membranes, these parameters do not directly influence the Knudsen number. The Knudsen number is defined strictly as the ratio between the molecular mean free path (λ) and the pore diameter (dp), and therefore depends only on temperature, pressure, and the characteristic pore size. Variations in porosity and membrane thickness modify the effective permeance, pressure drop, and relative contributions of viscous and Knudsen flow, while gas viscosity determines the magnitude of the continuum (Poiseuille) component. However, these factors do not alter the fundamental ratio λ/dp and therefore cannot change the Knudsen regime classification. Instead, they influence the transport resistance, flow dominance between mechanisms, and effective permeability, while Kn remains determined solely by λ and dp.

2.6 Safety and Reliability Considerations

Gas handling operations were conducted in a ventilated laboratory equipped with appropriate safety interlocks and leak detectors. Hydrogen was purged with inert gas after each run to prevent accumulation. Pressure lines and fittings were leak tested prior to every experiment, and all temperature zones were monitored continuously to maintain stable conditions throughout data acquisition.

* Corresponding to: M. M. Ramalan (email: mukramaramalan@gmail.com)
DOI: https://doi.org/10.11113/jamst.v30n1.335

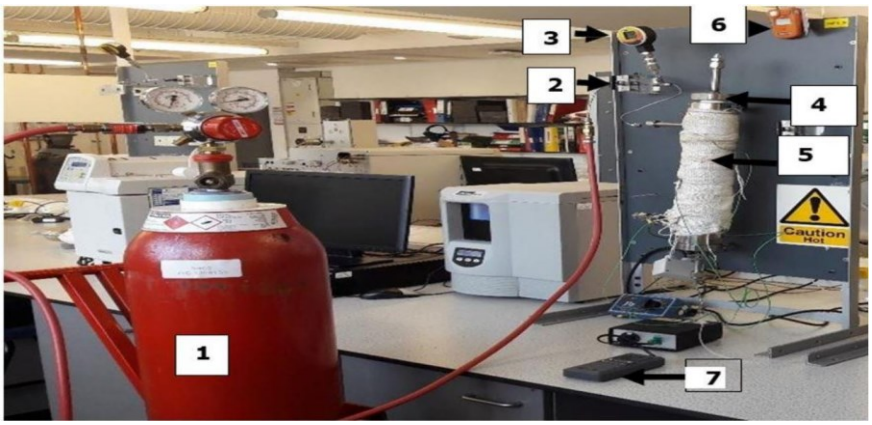

Figure 1a. Experimental setup for Knudsen number measurements: (1) compressed gas cylinder and regulator, (2) high pressure line, (3) inlet pressure gauge, (4) membrane holder, (5) heating jacket, (6) outlet gauge and relief valve, (7) data-acquisition unit

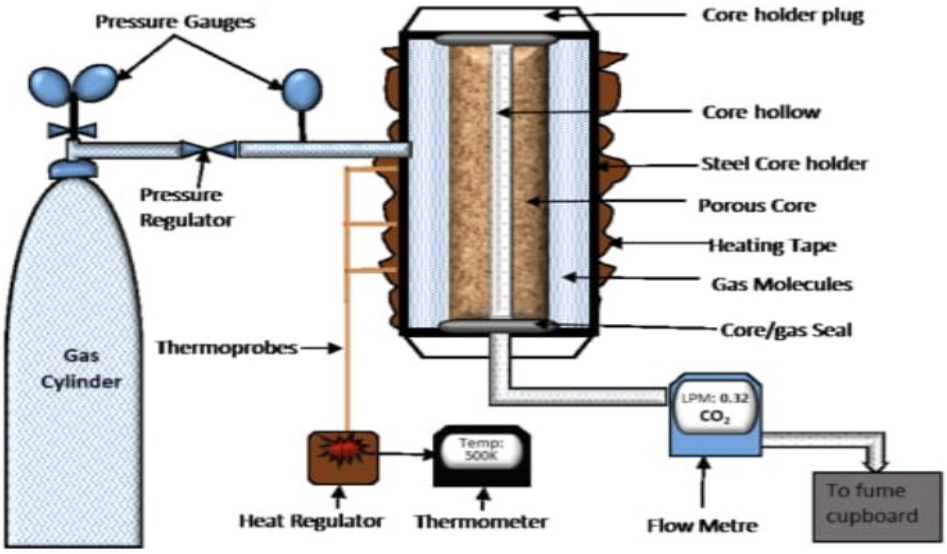

Figure 1b. Schematic of the membrane core-holder assembly and gas flow path used in the permeation experiments

2.7 Scanning Electron Microscopy (SEM) Characterisation

Samples were analysed for surface morphology and elemental composition using a Zeiss Evo LS10 Scanning Electron Microscope (SEM).

Prior to imaging, each membrane was sputter-coated with a thin layer of gold–palladium (approximately 10 nm) to prevent surface charging. Imaging was conducted under high vacuum at an accelerating voltage of 15 kV.

Representative micrographs are shown in Figure 2(a–b). The 15 nm membrane exhibits a densely packed top layer with fine, uniformly distributed nano pores and limited inter particle voids, characteristic of a well sintered micro porous surface. The 200 nm membrane displays a mesoporous texture with interconnected channels and moderate

* Corresponding to: M. M. Ramalan (email: mukramaramalan@gmail.com)
DOI: https://doi.org/10.11113/jamst.v30n1.335

roughness, forming continuous diffusion pathways that facilitate gas permeation. The 6000 nm support reveals a macroporous framework with large, irregular openings and thin inter-grain necks, producing a highly permeable structure but relatively lower surface area.

This progressive increase in pore diameter from micro to macro scale confirms the graded porous structure of the multi-layer membranes. The morphological variations observed by SEM align with the permeability and Knudsen-number trends discussed in later sections: smaller pores restrict molecular motion and promote surface interactions, whereas larger pores support continuum type flow. Moreover, differences in surface roughness and pore connectivity directly influence the wettability behaviour measured by contact angle analysis (Section 3.5), where finer pores exhibit greater hydrophilicity due to higher surface energy

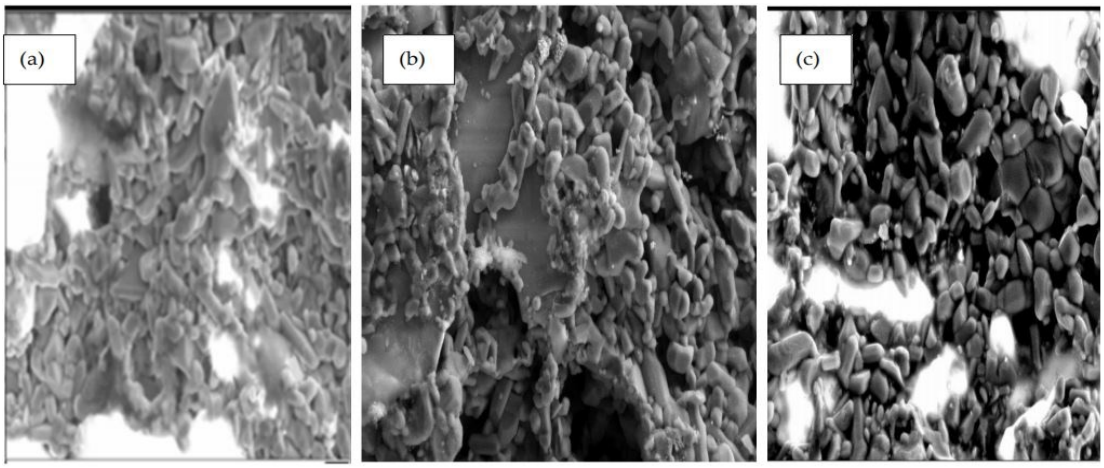

Figure 1. SEM micrographs of ceramic membrane supports with nominal pore diameters of (a) 15 nm, (b) 200 nm, and (c) 6000 nm. Scale bars: 1 µm

2.8 Contact Angle Measurement

Contact angle measurements were conducted to evaluate the dynamic and equilibrium wetting behaviours of the membrane supports and to understand the influence of surface energy on transport phenomena. The measurement provides insight into the degree of hydrophilicity or hydrophobicity, which determines the strength of liquid solid interactions and affects molecular adsorption, diffusion, and capillary flow within porous ceramic membranes.

The tests were performed using a One Attension ThetaLite optical tensiometer equipped with a high-speed camera operating at 51 frames per second (fps). Each membrane specimen (nominal pore sizes 15 nm, 200 nm, and 6000 nm) was cleaned with analytical grade isopropanol and dried at 60 °C for 1 hour before testing to remove any organic residue and ensure surface uniformity. A 5.0 µL droplet of distilled water was gently deposited using a micro-syringe onto the horizontal membrane surface under ambient conditions (25 ± 1 °C). Distilled water was selected for its well-known surface tension (72.8 mN/m at 25 °C) and consistent behaviour in sessile-drop testing.

* Corresponding to: M. M. Ramalan (email: mukramaramalan@gmail.com)
DOI: https://doi.org/10.11113/jamst.v30n1.335

High speed images were captured at 0.11 s, 0.21 s, and 0.46 s following droplet deposition to monitor the transient spreading process. The dynamic contact angle (θ_t) was determined by fitting the droplet contour using the Young–Laplace equation, and the quasi-static angle at 0.46 s was considered the equilibrium value (θ_e). Measurements were performed at three randomly selected points on each sample (n = 3), and the mean ± standard deviation is reported. Calibration of the camera, baseline, and lighting was carried out prior to each session to reduce parallax and reflection errors.

The contact angle evolution showed that the 15 nm support had the fastest reduction in θ_t, with angles decreasing from approximately 72° at 0.11 s to 59.8° ± 1.2° at 0.46 s. The 200 nm support exhibited moderate spreading (θ_e = 70.1° ± 1.8°), while the 6000 nm support maintained a nearly hemispherical droplet throughout the observation period (θ_e = 92.8° ± 2.3°). These results indicate a clear dependence of surface wettability on pore size: smaller pores exhibit higher surface energy and stronger capillary forces, promoting liquid spreading and adsorption. The larger pores of the 6000 nm support reduce the effective surface roughness and solid–liquid contact area, resulting in a lower adhesion energy and slight hydrophobicity ($\theta > 90°$).

This behaviour aligns with Wenzel and Cassie–Baxter wetting models, where rough, hydrophilic surfaces amplify wetting ($\theta < 90°$), while smoother or chemically neutral surfaces suppress spreading. For porous ceramics, this also correlates with capillary pressure, which scales inversely with pore radius ($\Delta P = 2\gamma\cos\theta / r_p$). Thus, the smaller pores (15 nm) develop stronger capillary suction, resisting liquid permeation but enhancing adsorption interactions that influence gas transport and Knudsen diffusion in later experiments.

Table 1 presents the averaged equilibrium contact angles for the three membranes, and representative frames are shown in Figure 3. Overall, the 15 nm and 200 nm supports are distinctly hydrophilic ($\theta < 90°$), while the 6000 nm support is marginally hydrophobic. These results substantiate the morphological observations from SEM and confirm that surface wettability and pore size are interlinked factors governing molecular interaction and flow behaviour across the membrane structure.

Table 1. Average equilibrium contact angles (mean ± SD, n = 3 at 0.46 s)

Support (nominal pore)	Contact angle (^{0})
15 nm	59.8±1.2
200 nm	70.1±1.8
6000 nm	92.8 ±2.3

* Corresponding to: M. M. Ramalan (email: mukramaramalan@gmail.com)
DOI: https://doi.org/10.11113/jamst.v30n1.335

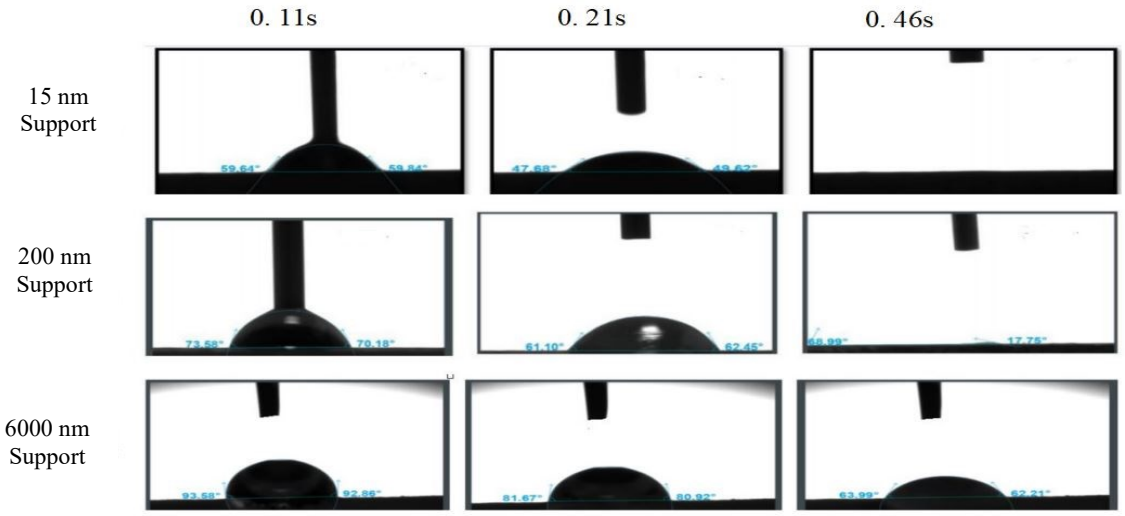

Figure 3. Time resolved contact angle images for (a) 15 nm, (b) 200 nm, and (c) 6000 nm membrane supports at 0.11 s, 0.21 s, and 0.46 s after droplet deposition. Conditions: distilled water, 5 µL droplet, 51 fps acquisition, ambient temperature 25 °C

2.8.1 Uncertainty and Regression Analysis

Experimental data always contain a degree of uncertainty arising from the accuracy of the measuring instruments, environmental fluctuations, and the data-reduction process. In this study, The principal sources of uncertainty originated from the measurement instruments described in Section 2.3, including the pressure transducers (±1.5 %), flow meters (±2 %), and temperature controller (±0.5 %). The propagation of these uncertainties through the Knudsen number calculation was estimated using the root sum square (RSS) method, which combines independent uncertainties of each measured parameter. Based on this analysis, the overall uncertainty in the computed Kn values did not exceed ±4.8 %, indicating that the experimental system was stable and repeatable within acceptable engineering limits.

To quantify the strength and reliability of the observed relationships, linear regression analysis was performed on the variation of Knudsen number (Kn) with transmembrane pressure (P) for each gas species and membrane pore size. The resulting coefficients of determination (R^2) ranged between 0.88 and 0.91, demonstrating a strong inverse correlation between Kn and P across the entire operating range of 20 – 300 kPa. Hydrogen exhibited the steepest regression slope (−0.70 Kn kPa^{-1}), followed by CO_2 (−0.54 Kn kPa^{-1}) and air (−0.37 Kn kPa^{-1}). These gradients are consistent with theoretical predictions based on molecular mean free path, confirming that lighter gases possess higher sensitivity to pressure change within the transition flow regime.

Residual plots indicated no systematic bias, suggesting that the experimental errors were random and normally distributed. Replicate measurements taken at constant pressure showed a standard deviation below 2.5 %, confirming the good repeatability of the tests. Consequently, the uncertainties do not significantly affect the observed linearity or the derived transport correlations. The following section discusses how these validated results relate to overall gas-transport behaviour in the composite ceramic membrane.

* Corresponding to: M. M. Ramalan (email: mukramaramalan@gmail.com)
DOI: https://doi.org/10.11113/jamst.v30n1.335

3.0 RESULTS AND DISCUSSION

3.1 Knudsen Number Behaviour with Transmembrane Pressure Hydrogen

Figure 4 illustrates the variation of the Knudsen number (Kn) with transmembrane pressure for hydrogen gas across membrane layers with nominal pore diameters of 15 nm, 200 nm, and 6000 nm. In all cases, Kn decreases progressively with increasing pressure, consistent with the pressure dependent reduction in molecular mean free path predicted by kinetic theory. This monotonic behaviour reflects the gradual shift from strongly rarefied conditions toward slip continuum transport as gas density increases.

The 15 nm selective layer exhibits the highest Kn values, described by the regression:

$$Kn=-2\times10-5P+6.9726\ (R2=0.8875)$$

The large intercept confirms that hydrogen transport in this nanoscale layer remains strongly rarefied even at elevated pressures, owing to the high degree of molecular confinement. The relatively steep negative slope indicates that Kn is highly sensitive to pressure changes in this layer, although the transport mechanism stays firmly within the rarefied regime across the entire 20–300 kPa range. The 200 nm mesoporous layer shows a weaker dependence on pressure, following:

$$Kn=-1\times10-6P+0.5229\ (R2=0.8875)$$

The smaller intercept places this layer within the transition to slip regime. The notably lower slope magnitude reflects reduced dominance of gas–wall interactions as the pore size increases, causing pressure to exert a more moderate influence on molecular rarefaction. The 6000 nm macroporous support yields the lowest Kn values, described by:

$$Kn=-4\times10-7P+0.0174\ (R2=0.8875)\backslash$$

Across the entire pressure range, Kn remains far below 0.1, confirming that this layer operates predominantly under continuum or slip-enhanced viscous flow. The extremely small slope demonstrates that pressure has minimal influence on rarefaction in this highly open pore structure, where molecular collisions overwhelmingly dominate over gas–wall interactions.

Although the three layers exhibit identical coefficients of determination ($R^2 = 0.8875$), their slopes and intercepts differ by more than an order of magnitude. This highlights the layer-specific nature of pressure-driven rarefaction in multilayer ceramic membranes. The combined behaviour confirms that hydrogen transport through the membrane cannot be represented by a single Kn–pressure correlation; rather, it emerges from a hierarchical sequence of rarefied, transitional, slip, and continuum regimes defined by the graded pore architecture.

* Corresponding to: M. M. Ramalan (email: mukramaramalan@gmail.com)
DOI: https://doi.org/10.11113/jamst.v30n1.335

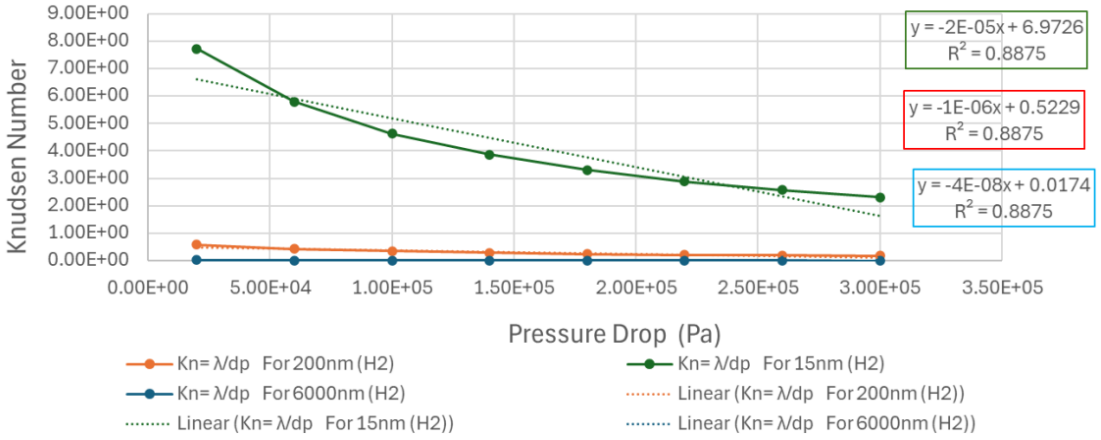

Figure 4. Variation of Knudsen number (Kn) with transmembrane pressure for Hydrogen across ceramic membranes with pore diameters of 15 nm, 200 nm, and 6000 nm at 100 °C

Figure 5 illustrates the dependence of the Knudsen number (Kn) on transmembrane pressure for carbon dioxide across membrane layers with pore diameters of 15 nm, 200 nm and 6000 nm. As with hydrogen, Kn decreases systematically with increasing pressure, consistent with the inverse pressure dependence of the molecular mean free path. However, CO_2 exhibits noticeably lower Kn values than hydrogen for all pore sizes due to its larger molecular diameter and higher molecular mass, which reduce the mean free path even at low pressure.

The regression analysis confirms linear Kn–pressure behaviour across the entire 20–300 kPa range, with all layers showing $R^2 = 0.8875$, indicating strong internal consistency in the experimental dataset. Despite identical R^2 values, the slopes and intercepts differ substantially, reflecting the different rarefaction levels in each layer.

For the 15 nm selective layer (green line), the fitted relation:

$$Kn = -1\times10^{-5}\,P + 5.3476\ (R^2 = 0.8875)$$

exhibits the steepest slope and the highest intercept, demonstrating that CO_2 transport in this layer begins within the transitional rarefied regime at low pressures. However, the magnitude of both parameters is lower than for hydrogen, confirming the reduced mean free path of CO_2. As pressure rises, Kn decreases rapidly, indicating accelerated transition toward slip flow due to increased CO_2 wall and CO_2–CO_2 collision frequency in the nanoscale pores.

The 200 nm intermediate layer follows the relation:

$$Kn = -1\times10^{-6}\,P + 0.4011\ (R^2 = 0.8875)$$

with a slope an order of magnitude smaller than in the 15 nm layer. This reflects a regime in which CO_2 is already close to slip flow even at low pressures. The moderate intercept confirms that rarefaction effects are weaker than in the selective layer but still non-negligible in the lower pressure range.

* Corresponding to: M. M. Ramalan (email: mukramaramalan@gmail.com)
DOI: https://doi.org/10.11113/jamst.v30n1.335

In the 6000 nm support layer (blue line), the behaviour is described by:

$Kn = -3\times10^{-8} P + 0.0134$ ($R^2 = 0.8875$).

The very small slope and intercept indicate that CO_2 transport in this macroporous region is essentially continuum-dominated across the full pressure range, with only minimal rarefaction effects observable. The Kn values here remain well below 0.01, consistent with classical continuum gas transport.

The comparative behaviour of the three layers highlights the strong dependence of CO_2 rarefaction on pore size. While hydrogen showed substantial rarefaction in both the 15 nm and 200 nm layers, CO_2 transitions more rapidly to slip and continuum flow as pressure increases. This is expected given its larger kinetic diameter (0.33 nm) and higher molecular mass (44 g mol^{-1}), both of which shorten the mean free path. The combination of lower Kn values, shallower slopes and reduced layer-to-layer contrast compared with hydrogen confirms that CO_2 is far less sensitive to pressure variations in nanoscale pores.

These results demonstrate how gas-specific molecular properties govern rarefaction behaviour in multilayer ceramic membranes, emphasising the need for pore-size optimisation when designing membranes for CO_2 separation, catalytic processing or mixed gas environments.

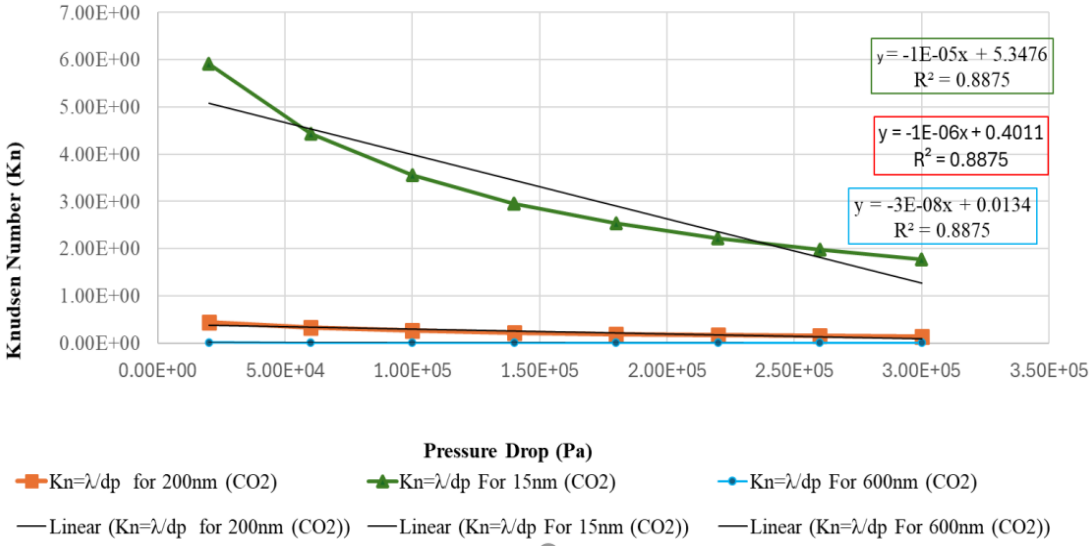

Figure 5. Variation of Knudsen number (Kn) with transmembrane pressure for carbon dioxide across ceramic membranes with pore diameters of 15 nm, 200 nm, and 6000 nm at 100 °C

Figure 6 presents the variation of the Knudsen number (Kn) with transmembrane pressure for air across the membrane layers of 15 nm, 200 nm and 6000 nm at 100 °C. Similar to hydrogen and carbon dioxide, Kn decreases monotonically with rising pressure, reflecting the contraction of the molecular mean free path as gas density increases. However, air exhibits the lowest Kn values and the weakest pressure sensitivity among the three gases studied, highlighting its limited susceptibility to rarefaction effects in nanoscale

* Corresponding to: M. M. Ramalan (email: mukramaramalan@gmail.com)
DOI: https://doi.org/10.11113/jamst.v30n1.335

ceramic membranes. The regression fits in Figure 6 show consistent linear behaviour, with all three layers yielding $R^2 = 0.8875$, confirming high repeatability and stable transitions across the pressure domain. Despite the identical R^2 values, each layer's slope and intercept differ significantly, illustrating the pore size dependent nature of air transport.

For the 15 nm selective layer (green line), the regression expression:

$$Kn = -9\times10^{-6}\,P + 3.6397\ (R^2 = 0.8875)$$

reveals a moderate intercept and a slope lower in magnitude compared with hydrogen or CO_2 in the same layer. This indicates that although air enters the lower transitional regime at low pressures, the degree of rarefaction is limited. As pressure increases, air transitions more quickly toward slip flow due to its relatively short mean free path, governed by the molecular characteristics of nitrogen and oxygen.

In the 200 nm intermediate layer (orange line), the relationship:

$$Kn = -7\times10^{-7}\,P + 0.273\ (R^2 = 0.8875)$$

captures the reduced rarefaction effects. The Kn values remain low across the entire pressure range, indicating that air operates primarily in the slip-flow regime. The slope is an order of magnitude smaller than in the 15 nm layer, showing that the influence of pressure on air's rarefied behaviour rapidly diminishes as the pore size increases.

The 6000 nm support layer (blue line) displays the weakest sensitivity overall, described by:

$$Kn = -2\times10^{-8}\,P + 0.0091\ (R^2 = 0.8875).$$

Here, Kn remains far below 0.01, well within the continuum regime. The minimal slope indicates that pressure has almost no influence on the rarefaction level at this pore scale, consistent with classical continuum gas dynamics where molecular collisions dominate over molecule wall interactions.

This hierarchy of behaviour reflects the composite nature of air, consisting mainly of N_2 and O_2, both having larger molecular diameters (0.364 nm and 0.346 nm) and higher collision frequencies compared with hydrogen. Consequently, air has the shortest mean free path among the gases studied, producing lower Kn values even in the smallest pores. These molecular properties explain why air shows the weakest Kn–pressure dependency, the shallowest slopes, and the earliest transition to continuum behaviour as pore size increases.

Overall, the air transport results reinforce the strong dependence of rarefaction on both molecular characteristics and pore geometry. Together with the hydrogen and CO_2 results, Figure 6 highlights the necessity of gas specific and pore scale specific modelling to accurately describe transport in composite ceramic membranes, particularly for applications such as gas separation, catalytic membrane processes, and mixed-gas permeation environments.

* Corresponding to: M. M. Ramalan (email: mukramaramalan@gmail.com)
DOI: https://doi.org/10.11113/jamst.v30n1.335

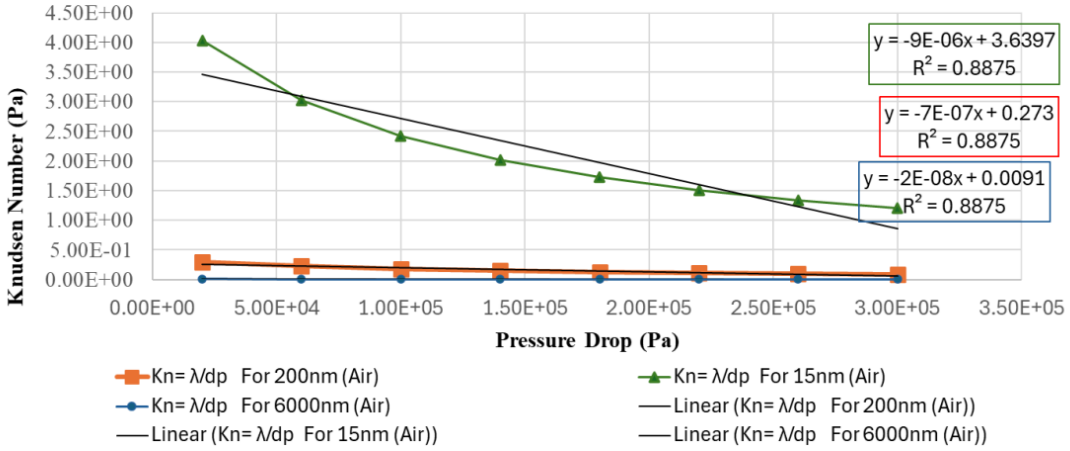

Figure 6. Variation of Knudsen number (Kn) with transmembrane pressure for Air across ceramic membranes with pore diameters of 15 nm, 200 nm, and 6000 nm at 100 °C

The consistent ordering of sensitivity (H_2 > CO_2 > air) highlights the dominance of molecular size and mass in determining how pressure variations influence gas transport in confined geometries. These observations further demonstrate that the selective layer retains strong rarefaction effects even under elevated pressures, compared with the significantly less responsive support layers.

3.2 Influence of Pore Architecture and Surface Characteristics

The graded structural design of the ceramic membrane plays a decisive role in shaping the observed Knudsen behaviour across all gases. The 15 nm selective layer, characterised by high surface area and densely interconnected nanopores, facilitates frequent gas–wall collisions, thereby amplifying rarefaction-dominated transport. This behaviour is further strengthened by the intrinsic surface chemistry of alumina: its hydrophilic nature and nanoscale surface roughness enhance adsorption interactions and increase the probability of molecule–wall momentum exchange.

As the pore diameter increases, the frequency of molecule–wall collisions decreases, allowing transport to shift progressively toward continuum dominated behaviour. The 200 nm intermediate layer therefore exhibits a hybrid response in which both rarefied and continuum mechanisms coexist, whereas the 6000 nm support layer operates almost entirely under continuum flow conditions. The progressive reduction in Kn sensitivity across these layers demonstrates a pore-size–stratified transport system, wherein each layer contributes a distinct flow regime: rarefied transport in the nanoporous surface layer, transitional flow in the mesoporous intermediate region, and low resistance continuum transport in the macroporous support.

Beyond Kn behaviour alone, the membrane's pore architecture influences pressure distribution and overall transport resistance. Variations in layer thickness, porosity, and surface roughness modify local velocity gradients and determine how the total pressure drop is partitioned across the membrane. Although these morphological characteristics do not change the definition of Kn, they directly affect the dominant resistance pathway. Under practical operating conditions, the 15 nm selective layer governs separation

* Corresponding to: M. M. Ramalan (email: mukramaramalan@gmail.com)
DOI: https://doi.org/10.11113/jamst.v30n1.335

performance, while the underlying support layer is engineered to minimise backpressure and ensure mechanical stability during operation.

3.3 Comparison with Theoretical Expectations and Literature Reports

The experimental trends obtained in this study closely reflect the fundamental predictions of kinetic gas theory, particularly the inverse relationship between molecular mean free path and pressure. As pressure increases, the mean free path decreases, yielding a corresponding reduction in Knudsen number an effect clearly observed across all tested gases and pore scales. The near linear Kn pressure relationships recorded experimentally are consistent with theoretical and computational studies of rarefied gas transport in micro and nanoporous media, which describe a gradual shift from molecule–wall dominated dynamics at high Kn to continuum dominated flow at low Kn.

Moreover, the attenuation of Kn sensitivity with increasing pore diameter aligns well with classical nanopore modelling literature. Studies of gas transport in porous materials consistently show that effective diffusivity, wall molecule interaction frequency, and momentum accommodation effects diminish as the system transitions from the transitional regime toward the continuum limit. The relative differences observed experimentally among hydrogen, carbon dioxide, and air correspond directly to their respective molecular diameters and collision cross-sections a trend widely reported in rarefaction theory and molecular kinetic simulations.

3.3.1 Data Validation against Theoretical Correlations

To further verify the reliability of the measured Kn pressure behaviour, the experimental results were compared with predictions from classical rarefied-gas transport theory. Mean free path values were calculated using the kinetic-theory expression previously defined in Equation (2), and theoretical Kn values were then obtained from the relation $Kn=\lambda/dp$. These theoretical curves exhibit the same inverse dependence on pressure and comparable linearity to the experimental trends, confirming that both the magnitude and slope of the measured Kn values fall within the expected range for transitional and slip flow regimes.

A qualitative comparison with composite models such as the Bosanquet formulation and with the conceptual framework of the Dusty Gas Model also indicates consistency: for large pores (6000 nm), continuum behaviour becomes dominant and the experimental Kn values approach first principles predictions, whereas for nanoscale pores (15 nm), enhanced wall interaction effects yield the higher Kn values expected for rarefied conditions. Although full DGM fitting is beyond the scope of this work, the close agreement between experimental results and kinetic-theory predictions provides strong validation for the accuracy and physical reliability of the measured Kn–pressure relationships.

Taken together, these findings substantiate established theoretical expectations while extending them to a multilayer ceramic membrane featuring distinct pore classes. The agreement between theoretical predictions and experimental slopes indicates that the membrane's graded pore structure produces a predictable and controllable progression of transport regimes. This reinforces recent efforts in the membrane research community to engineer nanostructured materials that deliberately maintain transitional, slip, or continuum behaviour according to functional requirements.

* Corresponding to: M. M. Ramalan (email: mukramaramalan@gmail.com)
DOI: https://doi.org/10.11113/jamst.v30n1.335

3.4 Gas Property Effects on Transport Regimes

The differing degrees of pressure sensitivity among hydrogen, carbon dioxide, and air arise primarily from intrinsic molecular properties, including molecular diameter, mass, and resulting mean free path. Hydrogen, possessing the smallest kinetic diameter (0.289 nm) and lowest molecular mass, naturally exhibits the longest mean free path under identical conditions. This produces the highest Kn values across all pore sizes, with particularly strong rarefaction effects in the 15 nm layer, where Kn falls firmly within the transitional regime at lower pressures. The steep Kn–pressure gradient for hydrogen highlights how strongly light gases respond to confinement and wall interactions when transported through nanoscale pores.

Carbon dioxide, with a larger kinetic diameter (0.330 nm) and higher molecular mass, displays intermediate Kn values and correspondingly moderate sensitivity to pressure. Its behaviour is consistent with the expected scaling between molecular diameter and mean free path, and its decline in Kn with pressure resembles theoretical rarefaction curves observed in molecular simulation studies.

Air exhibits the smallest Kn values and the shallowest Kn pressure slope across all layers. As a mixed gas dominated by nitrogen and oxygen both larger and heavier than hydrogen its mean free path is shorter, resulting in earlier onset of slip and continuum behaviour. Even in the 15 nm layer, air remains near the lower boundary of the transitional regime, while the 200 nm and 6000 nm layers operate well within slip and continuum conditions, respectively.

These molecular scale dependencies underscore the importance of aligning membrane operating conditions with gas properties. Membranes intended for hydrogen purification, for example, must account for the stronger rarefaction sensitivity of hydrogen and may benefit from maintaining pressures where transitional flow enhances selective transport.

3.5 Implications for Membrane Engineering and Process Integration

The pore size stratified Kn behaviour observed in this study has significant implications for the engineering of advanced ceramic membranes. The 15 nm selective layer, operating mainly within the transitional flow regime, is particularly sensitive to molecular properties and is therefore highly relevant for applications requiring mass discrimination, such as hydrogen purification or isotopic separation. The transitional regime enhances selectivity by amplifying molecule wall collisions and differences in molecular diffusivity.

The 200 nm intermediate layer serves as a bridging zone between rarefied and continuum flows. Its mixed mode behaviour provides a stabilising influence, distributing pressure gradients across the membrane while preventing abrupt regime transitions that could otherwise produce flow instabilities or localised transport resistances.

The 6000 nm support layer is engineered for low flow resistance and mechanical integrity. Operating firmly within the continuum regime, it ensures minimal contribution to Knudsen resistance and prevents excessive backpressure that could compromise both separation performance and structural durability.

From a process integration standpoint, the measured dependence of Kn on pressure demonstrates that system pressure can be used as a tunable control parameter. By selecting an appropriate operating pressure, designers can shift the selective layer into the desired

* Corresponding to: M. M. Ramalan (email: mukramaramalan@gmail.com)
DOI: https://doi.org/10.11113/jamst.v30n1.335

transport regime transitional for enhanced selectivity, or slip/continuum for enhanced flux while relying on the support layer to maintain flow stability. The ability to combine multiple flow regimes within a single membrane suggests opportunities for hybrid membrane systems that integrate rarefied and continuum characteristics in a single functional architecture.

Such multi regime transport behaviour is advantageous in hydrogen purification, CO_2 capture, catalytic membrane reactors, and ammonia synthesis, where both selectivity and permeability must be carefully balanced.

4.0 SUMMARY AND OUTLOOK

This study systematically examined the sensitivity of the Knudsen number to transmembrane pressure in multilayer alumina membranes comprising 15 nm, 200 nm, and 6000 nm pore layers. Experiments conducted with hydrogen, carbon dioxide, and air at 100 °C over a pressure range of 20–300 kPa revealed the expected inverse relationship between Kn and pressure. Increasing pressure reduces the molecular mean free path, thereby shifting gas transport from rarefied to transitional, slip, or continuum regimes depending on pore size. Hydrogen displayed the greatest $\Delta Kn/\Delta P$ owing to its small kinetic diameter and long mean free path, whereas carbon dioxide and air exhibited lower sensitivities. The linearity of the experimental relationships ($R^2 \approx 0.88$) and an uncertainty analysis of ±4–5 % confirm the robustness of the measurements. SEM imaging validated the graded membrane architecture, and contact-angle measurements showed reduced hydrophilicity with increasing pore size, affecting the intensity of gas–wall interactions under rarefied conditions.

All measurements were performed at a fixed temperature of 100 °C (373 K) to isolate the effects of pressure and structural confinement on Knudsen-number behaviour. Although the molecular mean free path scales with temperature as $\lambda \propto T/P$, altering temperature would also modify gas viscosity, molecular thermal velocity, and surface adsorption characteristics. Such coupled thermophysical changes would complicate interpretation of pressure-dependent trends and hinder mechanistic comparisons among the three membrane layers. Maintaining a constant temperature therefore ensures that observed variations in Kn arise solely from pressure and pore-scale geometry. Nonetheless, the temperature dependence of rarefied gas transport remains an important aspect of Knudsen and transitional flow theory. Future work will extend the present dataset to a broader temperature range to quantify how thermal effects influence rarefaction behaviour, surface accommodation, and the relative contributions of viscous and Knudsen mechanisms in multilayer ceramic membranes.

Outlook: Future studies should extend these measurements to mixed-gas feeds, wider temperature ranges, and higher pressures to approximate industrial operating environments. Additional characterisation such as porosimetry, BET analysis, and surface roughness measurements would improve correlations between morphology and flow regime distributions. Integrating the present findings with multiscale modelling such as slip-corrected continuum models, Lattice Boltzmann methods, or hybrid DSMC–CFD frameworks would expand predictive capabilities across transitional regimes. Further evaluation under cyclic loading, elevated flow rates, and functionalised or catalytic

* Corresponding to: M. M. Ramalan (email: mukramaramalan@gmail.com)
DOI: https://doi.org/10.11113/jamst.v30n1.335

surfaces would provide insights into long-term performance and expand applications in hydrogen purification, CO_2 capture, and catalytic membrane reactors.

5.0 CONCLUSION

This study provides a comprehensive experimental assessment of how the Knudsen number responds to changes in transmembrane pressure within multilayer ceramic membranes featuring pore diameters of 15 nm, 200 nm, and 6000 nm. Across all three gases tested hydrogen, carbon dioxide, and air a robust inverse relationship between Kn and pressure was observed, consistent with reductions in molecular mean free path at elevated pressures. Hydrogen demonstrated the largest sensitivity to pressure owing to its small kinetic diameter, while CO_2 and air exhibited progressively weaker dependence. These experimental findings were supported by theoretical calculations of mean free path and Knudsen diffusion coefficients, and by statistical correlations ($R^2 \approx 0.88$).

Surface and structural characterisation revealed the mechanistic basis for these trends: the 15 nm layer, with its high surface area and hydrophilic character, enhances gas–wall interactions and contributes significantly to rarefaction-driven resistance; by contrast, the 6000 nm macroporous layer operates near the continuum limit and contributes minimally. By stacking these layers, the membrane effectively integrates multiple transport regimes, enabling a tunable balance between selectivity, permeability, and mechanical support.

The results not only provide validated experimental benchmarks for modelling rarefied gas flow but also offer a conceptual framework for designing multilayer ceramic membranes tailored to hydrogen purification, CO_2 separation, and catalytic membrane reactors. These insights will facilitate the development of next-generation nanostructured membrane systems with optimised performance across a wide range of operating conditions.

DECLARATION OF COMPETING INTEREST

The authors declare that there are no conflicts of interest related to the publication of this paper. All experimental data, interpretations, and conclusions were conducted and presented independently without any financial or personal bias.

ACKNOWLEDGEMENTS

The authors gratefully acknowledge the support provided by Robert Gordon University and Petroleun Training Development fund (PTDF) for access to experimental facilities, instrumentation, and technical guidance throughout this research. Their assistance was invaluable in the successful completion of this work. The authors also extend appreciation to colleagues who contributed to discussions and practical insights during the membrane testing and data analysis phases. No external funding was received for this study.

REFERENCES

[1] Bera, A., Kumar, S., Foroozesh, J., & Gharavi, A. (2022). Multiphysics gas transport in nanoporous unconventional reservoirs: Challenges of mathematical modelling.

* Corresponding to: M. M. Ramalan (email: mukramaramalan@gmail.com)
DOI: https://doi.org/10.11113/jamst.v30n1.335

Journal of Natural Gas Science and Engineering, 103, 104649.
[2] Schlaich, A., Barrat, J. L., & Coasne, B. (2025). Theory and modeling of transport for simple fluids in nanoporous materials: From microscopic to coarse-grained descriptions. *Chemical Reviews, 125*(5), 2561–2624.
[3] Ogunlude, P. (2023). *Gas diffusion transport characteristics and mathematical description of membrane systems with application for biogas upgrading* (Doctoral dissertation, Robert Gordon University).
[4] Liu, Y., Li, N., Cui, X., Yan, W., Su, J., & Jin, L. (2022). A review on the morphology and material properties of the gas separation membrane: Molecular simulation. *Membranes, 12*(12), 1274.
[5] Armatas, G. S. (2006). Determination of the effects of the pore size distribution and pore connectivity distribution on the pore tortuosity and diffusive transport in model porous networks. *Chemical Engineering Science, 61*(14), 4662–4675.
[6] Kawashima, K., Shirzadi, M., Fukasawa, T., Fukui, K., Tsuru, T., & Ishigami, T. (2022). Numerical modeling for particulate flow through realistic microporous structure of microfiltration membrane: Direct numerical simulation coordinated with focused ion beam scanning electron microscopy. *Powder Technology, 410*, 117872.
[7] Maier, L., Scherle, M., Hopp-Hirschler, M., & Nieken, U. (2021). Effective transport parameters of porous media from 2D microstructure images. *International Journal of Heat and Mass Transfer, 175*, 121371.
[8] Vaartstra, G., Lu, Z., Grossman, J. C., & Wang, E. N. (2021). Numerical validation of the dusty-gas model for binary diffusion in low aspect ratio capillaries. *Physics of Fluids, 33*(12).
[9] Reinecke, S. A., & Sleep, B. E. (2002). Knudsen diffusion, gas permeability, and water content in an unconsolidated porous medium. *Water Resources Research, 38*(12), 16-1.
[10] Ishizaki, K., Komarneni, S., & Nanko, M. (2013). *Porous materials: Process technology and applications* (Vol. 4). Springer Science & Business Media.
[11] Mourkou, M., Yu, H., Baltussen, S., Snead, N., Kapil, N., & Coppens, M. O. (2024). A novel ultra-high vacuum diffusion setup to study Knudsen diffusion. *Reaction Chemistry & Engineering, 9*(11), 3047–3059.
[12] Kotobuki, M., Gu, Q., Zhang, L., & Wang, J. (2021). Ceramic–polymer composite membranes for water and wastewater treatment: Bridging the big gap between ceramics and polymers. *Molecules, 26*(11), 3331.
[13] Han, B., & Gabriel, J. C. P. (2024). Thin-film nanocomposite (TFN) membrane technologies for the removal of emerging contaminants from wastewater. *Journal of Cleaner Production, 480*, 144043.
[14] Xu, D., Luo, X., Jin, P., Zhu, J., Zhang, X., Zheng, J., Yang, L., Zhu, X., Liang, H., & Van der Bruggen, B. (2022). A novel ceramic-based thin-film composite nanofiltration membrane with enhanced performance and regeneration potential. *Water Research, 215*, 118264.
[15] Hu, J., Zhang, Y., & Dong, M. (2024). Recent advances in layered double hydroxides membranes: Insights into multiple mass transport. *Advanced Functional Materials, 34*(14), 2312452.
[16] Chaudhari, S., Chakravarty, S., Cho, Y., Seo, J., Shon, M., & Nam, S. (2025). Advancements in organic solvent nanofiltration: The critical role of polyamide

* Corresponding to: M. M. Ramalan (email: mukramaramalan@gmail.com)
DOI: https://doi.org/10.11113/jamst.v30n1.335

membranes in sustainable industrial applications. *Processes, 13*(7), 2212.
[17] Zhou, X., Shevate, R., Huang, D., Cao, T., Shen, X., Hu, S., Mane, A. U., Elam, J. W., Kim, J. H., & Elimelech, M. (2023). Ceramic thin-film composite membranes with tunable subnanometer pores for molecular sieving. *Nature Communications, 14*(1), 7255.
[18] Karim, S. S., Ahsan, M., Farrukh, S., Fan, X., & Yu, Z. (2025). Multi-layer Composite (MLC) membranes gas transport models and separation mechanisms. In *Multi-Layer Composite (MLC) Membranes for Gas Separation: Volume 1: A Fundamental Overview* (pp. 159–185). Springer Nature Switzerland.
[19] Oyama, S. T., Yamada, M., Sugawara, T., Takagaki, A., & Kikuchi, R. (2011). Review on mechanisms of gas permeation through inorganic membranes. *Journal of the Japan Petroleum Institute, 54*(5), 298–309.
[20] Guan, Z. L., Wang, Y. D., Wang, Z., Hong, Y., Liu, S. L., Luo, H. W., Liu, X. L., & Su, B. L. (2024). The synthesis, characteristics, and application of hierarchical porous materials in carbon dioxide reduction reactions. *Catalysts, 14*(12), 936.
[21] Abbassi, A., Moghaddam, M., & Ghazanfarian, J. (2022). Microstructure effects on performance and deactivation of hierarchically structured porous catalyst: A pore network model. *SSRN Electronic Journal*.
[22] Bhalani, D. V., & Lim, B. (2024). Hydrogen separation membranes: A material perspective. *Molecules, 29*(19), 4676.
[23] Zhang, Z., Zhou, W., Wang, T., Gu, Z., Zhu, Y., Liu, Z., Wu, Z., Zhang, G., & Jin, W. (2023). Ion–conducting ceramic membrane reactors for the conversion of chemicals. *Membranes, 13*(7), 621.
[24] Gu, Y. Q., Jin, Z., Zhang, H., Xu, R. J., Zheng, M. J., Guo, Y. M., Song, Q. S., & Jia, C. J. (2015). Transition metal nanoparticles dispersed in an alumina matrix as active and stable catalysts for COx-free hydrogen production from ammonia. *Journal of Materials Chemistry A, 3*(33), 17172–17180.
[25] Sabouri, R., Ladewig, B. P., & Prasetya, N. (2025). Mixed matrix membranes for hydrogen separation: A comprehensive review and performance analysis. *Journal of Materials Chemistry A*.
[26] Król, A., Gajec, M., Holewa-Rataj, J., Kukulska-Zając, E., & Rataj, M. (2024). Hydrogen purification technologies in the context of its utilization. *Energies, 17*(15), 3794.
[27] Biron, D. D. S., Poletto, P., Duarte, J., Zeni, M., Bergmann, C. P., & Santos, V. D. (2015). Preparation and characterization of PA66/alumina composite membrane. *Materials Research, 18*(4), 748–755.
[28] Biron, D. D. S., Poletto, P., Duarte, J., Zeni, M., Bergmann, C. P., & Santos, V. D. (2021). Preparation and characterization of PA66/alumina composite membrane. In *Ciência e Engenharia de Materiais: Conceitos, Fundamentos e Aplicação* (Vol. 1, pp. 338–354). Editora Científica Digital.
[29] Ha, J. H., Abbas Bukhari, S. Z., Lee, J., & Song, I. H. (2016). Preparation and characterisation of alumina-based composite support layers. *Advances in Applied Ceramics, 115*(4), 229–235.
[30] Li, T., Rabuni, M. F., Hartley, U. W., & Li, K. (2022). Advanced ceramic membrane design for gas separation and energy application. In *60 Years of the Loeb-Sourirajan Membrane* (pp. 239–268). Elsevier.

* Corresponding to: M. M. Ramalan (email: mukramaramalan@gmail.com)
DOI: https://doi.org/10.11113/jamst.v30n1.335

[31] Bhandari, A. R., Flemings, P. B., Ramiro-Ramirez, S., Hofmann, R., & Polito, P. J. (2019). Gas and liquid permeability measurements in Wolfcamp samples. *Fuel, 236*, 1026–1036.
[32] Zrelli, A., Bessadok, A., & Alsalhy, Q. (2022). Important parameters of ceramic membranes derived from oasis waste and its application for car wash wastewater treatment. *Journal of Membrane Science and Research, 8*(1), e247250.
[33] Wang, F., Lee, J., Ha, J. H., & Song, I. H. (2017). Surface modification of alumina membranes via a sol-gel process for antifouling properties. *Materials Letters, 191*, 200–202.
[34] Hashemi, T., Mehrnia, M. R., & Ghezelgheshlaghi, S. (2022). Influence of alumina nanoparticles on the performance of polyacrylonitrile membranes in MBR. *Journal of Environmental Health Science and Engineering, 20*(1), 375–384.
[35] Kageyama, H., Hayashi, K., Maeda, K., Attfield, J. P., Hiroi, Z., Rondinelli, J. M., & Poeppelmeier, K. R. (2018). Expanding frontiers in materials chemistry and physics with multiple anions. *Nature Communications, 9*(1), 772.

* Corresponding to: M. M. Ramalan (email: mukramaramalan@gmail.com)
DOI: https://doi.org/10.11113/jamst.v30n1.335